ALCHEMY Jurnal Penelitian Kimia

Official Website: https://jurnal.uns.ac.id/alchemy

ISSN 1412-4092
EISSN 2443-4183

The Influence of Solvent and Heating Time Toward the Percent Yield of Sumbermanjing Pyrophyllite-Polyethylene Glycol (PEG) 6000 Composites

Siti Mutrofin[a*], Ekantoro Ekantoro[a], Rurini Retnowati[a], Hanisah Kamilah[b,c]

[a]*Department of Chemistry, Faculty of Mathematics and Natural Sciences, Brawijaya University*
Jalan Veteran, Ketawanggede, Lowokwaru, Malang, Jawa Timur 65145, Indonesia
[b]*Department of Crop Science, Faculty of Agricultural and Forestry Science, Universiti Putra Malaysia*
Sarawak Campus, Bintulu, Sarawak, 97008,
[c]*Halal Product Research Institute, Universiti Putra Malaysia*
Serdang, Selangor, Malaysia

[*]*Corresponding author: mutrofin@ub.ac.id*

DOI: 10.20961/alchemy.22.1.104024.228-240

Received 13 June 2025, Revised 8 September 2025, Accepted 12 January 2026, Published 31 March 2026

Keywords:

composite;
polyethylene glycol;
pyrophyllite.

ABSTRACT. The synthesis of clay-polymer composites has attracted considerable interest due to their promising potential properties. The composites were prepared from Sumbermanjing pyrophyllite and polyethylene glycol (PEG) 6000. This research aims to evaluate the influence of solvent and heating time on the percent yield of the composites. Pyrophyllite-PEG composites were synthesized via the casting and sol-gel methods with variations in solvent (demineralized water, methanol, acetone) and heating time (1, 1.5, and 2 hours). The highest yield (37.7239%) was achieved by a composite synthesized with acetone and a 2-hour heating treatment. The composite prepared with demineralized water showed poorer PEG diffusion into the pyrophyllite structure than did those prepared with methanol or acetone. A 2-hour treatment produced a more uniform, relatively smaller porous structure, despite subtle differences across various heating conditions. Statistical analysis revealed a significant difference among solvent treatments, but no significant difference among heating times. The melting points of the 1-hour and 2-hour composites were 120.7667 °C and 116.0333 °C, respectively, suggesting a successful composite synthesis. The successful composite synthesis was further confirmed by Fourier Transform Infrared (FTIR) spectra, which showed characteristic functional groups (O–H stretching, 3673.92 cm^{-1}; C–H stretching, 2882.37 cm^{-1}; Al–OH stretching, 1146.67 cm^{-1}).

INTRODUCTION

Composite materials play an important role in technological development. Composite materials consist of two or more distinct materials to produce a new product with more enhanced characteristics, with various applications, such as bridges, car bodies, and biomedical (Callister and Rethwisch, 2020; Egbo, 2021). Clay-polymer composites are promising materials due to their advantages for various applications, including efficient removal of organic and inorganic contaminants (Amari *et al*., 2021). These composites are synthesized by combining clay minerals with polymers. The integrated polymer is absorbed onto the clay's surface. As the clay layers reassemble, an intercalated nanocomposite forms, with the polymer filling the interlayer gaps (Buruga *et al*., 2019). Pyrophyllite is an example of a clay mineral used extensively across various industries, including pesticides, paper, plastics, and pharmaceuticals, and serves as an alternative to feldspar in the fiberglass industry (Ali *et al*., 2021). This mineral mainly consists of Si (57.7%), Al (16.7%), K (20.6%), Fe (2.47%), Ti (2.33%), and Cu (0.088%), along with trace amounts of potassium oxide, vanadium oxide, and copper oxide occupying the interlayer space of pyrophyllite (Mutrofin *et al*., 2018). Structurally, pyrophyllite is composed of an octahedral layer with Al^{3+} coordinated to oxygen and hydroxyl (OH^-) interposed between two SiO_4 tetrahedral sheets containing Si^{4+} as the center of the tetrahedral layer structure (Essalhi *et al*., 2017; Wang *et al*., 2023). Indonesia has a vast abundance of pyrophyllite mineral deposits. The total estimated pyrophyllite in East Java alone is approximately 65000 tons. Argotirto area in Sumbermanjing Wetan sub-district, located in Malang regency

Cite this as: Mutrofin, S., Ekantoro, E., Retnowati, R., and Kamilah, H. (2026). The Influence of Solvent and Heating Time Toward the Percent Yield of Sumbermanjing Pyrophyllite-Polyethylene Glycol (PEG) 6000 Composites. *ALCHEMY Jurnal Penelitian Kimia*, 22(1), 228-240. doi: https://dx.doi.org/10.20961/alchemy.22.1.104024.228-240.

(Indonesia), hosts a potential pyrophyllite reserve (Martadiastuti *et al*., 2024). Given the extensive availability of pyrophyllite in this area, additional research is needed on its physical and chemical properties relevant to the synthesis of clay-polymer composites.

Polyethylene glycol (PEG) is a polymer composed of repeating ethylene oxide units with varying chain lengths and molecular weights, synthesized by ring-opening polymerization of ethylene oxide using methanol or water as the solvent (Gaballa *et al*., 2024). PEG is widely used across various industries due to its water-solubility, low melting point, non-toxicity, inertness, and high hydrophilicity (Bîrcă *et al*., 2019; Helsinta *et al*., 2021). The linear-chain structure of PEG 6000 can potentially intercalate into the clay interlayers, resulting in a robust clay-polymer composite. The presence of the PEG hydroxyl group supports this interaction. Furthermore, van der Waals interactions also facilitate intercalation, arising from the difference in electrical charge between the clay and the polymer (Et-tanteny *et al*., 2024). The abundance of pyrophyllite and its intercalation capability with PEG make it a potential candidate for clay-polymer composites. The casting method involves placing the liquid material into a shaped mold, allowing it to solidify, and then separating the mold (Krindli *et al*., 2021). The sol-gel technique involves transforming a colloidal solution into a gel with extensive surface coverage and is relatively economical. This technique works by mechanically stirring the solutions until homogeneous, followed by hydrolysis and polycondensation, with the excess solvent removed by evaporation and heating (Choundhury, 2024).

In this study, the effects of solvent and heating time variations on the synthesis of composites prepared by the casting and sol-gel methods were analyzed. Furthermore, the composites were characterized using Fourier Transform Infrared (FTIR) and melting-point analysis. This study is expected to promote the potential use of pyrophyllite and polyethylene glycol (PEG) in the development of clay-polymer composites.

RESEARCH METHODS

Equipment and Materials

The materials used in this research are pyrophyllite mineral from Sumbermanjing District, South Malang (Indonesia), commercial polyethylene glycol (PEG) 6000, demineralized water, Whatman 42 filter paper, baking paper, aluminum foil, methanol p.a (99.5%), and acetone p.a (99.5%), purchased from a local chemical supplier in Malang, Indonesia. The equipment and instruments used in this research include pestle and mortar (Onemed), analytical balance, 200 and 300 mesh sieves (Test Sieve), watch glass (Pyrex), magnetic stirrer (Thermo Scientific Cimarec) and magnetic stirrer bar (2 centimeters long) (Thermo Scientific Cimarec), petri dish (Herma), glass funnel (Pyrex), porcelain cup (Pyrex), furnace (Fisher Scientific Isotemp Muffle Furnace 550-14), melting point apparatus (Ivymen WRS-1B) and Fourier Transform Infrared Spectroscopy (FTIR) spectrophotometer (Shimadzu IR Spiri-T).

Preparation of Pyrophyllite Solution

The pyrophyllite was prepared by crushing 100 g of pyrophyllite into a fine powder using a mortar and pestle, followed by screening through 200- and 300-mesh sieves. The pyrophyllite was further calcined at 300 °C for 5 hours and washed with 200 mL of deionized water in an Erlenmeyer flask on a magnetic stirrer at 300 rpm for 45 minutes, then filtered through a Whatman 42 filter paper. The product was further dried in a furnace at 300 °C for 1 hour, then cooled in a desiccator. A total of 1.5 g of pyrophyllite was added to three separate 50 mL beakers, followed by the addition of 5 mL of the solvent (demineralized water, methanol, and acetone). The mixtures were stirred at room temperature using a magnetic stirrer at 900 – 1000 rpm for 1 hour. The same procedure was repeated three times for each solvent.

Preparation of PEG 6000 Solution

PEG solutions were prepared by adding 2 g of PEG 6000 into three separate 50 mL beakers, followed by 5 mL of each solvent (demineralized water, methanol, and acetone). These solutions were stirred at 900 – 1000 rpm for 1 hour using a magnetic stirrer to ensure uniform distribution. The procedure was also repeated three times for each solvent.

Composite Synthesis: Solvent Variation

The composites were prepared by adding the PEG solution to the pyrophyllite solution using the same solvent, resulting in a mixture. The mixtures were stirred at 900 – 1000 rpm for 3 hours. The weight of the petri dishes and the baking papers was measured using an analytical balance. The resulting solutions were placed on a

petri dish lined with baking paper and dried in an oven at 100 – 105 °C for 1.5 hours before being placed in a desiccator until completely dried. Among the solvent variations prepared, the one yielding the highest percent yield was used to determine the optimal heating duration for the composites.

Composite Synthesis: Heating Time Variation

The PEG solution was added to the pyrophyllite solution prepared with the selected solvent from the previous step. The mixtures were stirred at 900 – 1000 rpm for 3 hours before being placed on a petri dish lined with baking paper and dried in an oven at 100 – 105 °C for 1, 1.5, and 2 hours. The final composites were cooled off in a desiccator until dry. The same procedure was repeated three times for each solvent variation, and the percent yield for each was calculated to determine the yield of each sample.

Characterization Techniques

The selected composites were characterized by FTIR spectroscopy to identify their functional groups. A melting point apparatus was used to assess the thermal behavior of the composite samples. The thermal analysis commenced at 110 °C with a controlled heating rate of 1 °C/min. Both onset and completion temperatures were recorded by the instrument, indicating the temperature interval over which the sample transformed from the solid to the liquid phase. The measurement relies on the heat absorbed by the sample during the phase change. This transition temperature corresponds to the sample's melting point. The melting point of the samples was determined as the average of the initial and final temperatures during melting.

Data Analysis

IBM SPSS software was used to perform statistical analyses of the data, including ANOVA, T-tests, and Duncan Multiple-Range Test (DMRT). One-way ANOVA (Analysis of Variance) was performed to validate the effects of varying the solvent and heating duration using Equations 1 – 4.

$$CF = \frac{\left(\sum_{i=1}^{h}\sum_{j=1}^{n} Y_{ij}\right)^2}{h \times n} \quad (1)$$

$$SST = \sum_{i=1}^{h}\sum_{j=1}^{n} Y_{ij}^2 - CF \quad (2)$$

$$SSB = \sum_{i=1}^{h} \frac{\left(\sum_{j=1}^{n} Y_{ij}\right)^2}{n} - CF \quad (3)$$

$$\text{Sum of Squares Within groups (SSW)} = SST - SSB \quad (4)$$

Description:
CF = correction factor
SST = total sum of squares
SSB = sum of squares between groups
SSW = sum of squares within groups
Y = representing the percent yield value

The null hypothesis (H_o) and alternative hypothesis (H_1) were used to determine whether treatments differ significantly. The null hypothesis (H_0) states that varying the treatment within the sample has no difference in means. The alternative hypothesis (H_1) indicates that the means differ.

$F_{table} = 2.447$

If $F_{exp} > F_{table}$, H_0 is rejected, indicating a difference.

Duncan Multiple-Range Test (DMRT) is a post hoc test used to perform pairwise comparisons within each subset of means. This post hoc test compares d_{ij} with R_p to determine whether there is a significant difference, as shown in Equations 5 – 6.

$$R_p = r_{\alpha,p,v}\sqrt{\frac{MSE}{n}} \quad (5)$$

$$d_{ij} = \bar{X}_A - \bar{X}_B \quad (6)$$

Description:
R_p = the closest significant range value for comparison
$r_{\alpha,p,v}$ = studentized range statistic at a significance level of α, with p means and v degrees of freedom
MSE = mean square error from ANOVA

n = number of replicates from each group
d_{ij} = difference between two means
$\bar{X}_A, \bar{X}_B$ = sample means of treatments A and B
p = range from 2 to the number of means
v = degrees of freedom

The t-test is a statistical method for comparing the means of two groups. If $T_{exp} > T_{table}$ (the critical T value), then there is a significant difference between the groups. The critical T value can be found in the Student's T table. The calculation for Fisher's T-test to determine T_{exp} is shown in Equation 7.

$$t = \frac{\bar{X}_1 - \bar{X}_2}{\sqrt{\frac{S_1^2}{n_1} + \frac{S_2^2}{n_2}}} \quad (7)$$

Description:
$\bar{X}_1$ and $\bar{X}_2$ = means of each group
S_1^2 and S_2^2 = variances of each group
n_1 and n_2 = number of data in each group

RESULTS AND DISCUSSION

Percent Yield Data and Sample Observations

The percent yield was calculated by comparing the mass of the composites before and after heating, as shown in Equation 8.

$$\%\ \text{Yield} = \frac{X - Z}{Y - Z} \times 100\% \quad (8)$$

Description:
X = dried composite + petri dish + baking paper (g)
Y = wet composite + petri dish + baking paper (g)
Z = petri dish + baking paper (g)

Table 1. Percentage yield data on various solvents.

Sample	A	B	C	D	E	Yield (%)	Average yield (%)
W1	24.2508	36.0452	27.3073	11.7944	3.0565	25.9148	26.8195
W2	23.0803	33.6974	25.9955	10.6171	2.9152	27.4576	
W3	23.5022	34.6972	26.5345	11.195	3.0323	27.0862	
M1	23.2413	31.4952	26.0821	8.2539	2.8408	34.4177	34.7833
M2	24.191	31.9248	27.0447	7.7338	2.8537	36.8990	
M3	23.7966	33.0497	26.8532	9.2531	3.0566	33.0333	
Ac1	22.9664	31.6421	26.1192	8.6757	3.1528	36.3406	36.2680
Ac2	22.422	30.6741	25.4866	8.2521	3.0646	37.1372	
Ac3	22.707	30.6688	25.5196	7.9618	2.8126	35.3262	

*A = Total weight of the petri dish and baking paper, B = Total weight of the petri dish, baking paper and composites mixture before heating process, C = Total weight of the petri dish, baking paper and composite after heating process, D = B-A, showing the weight of the composites mixture, E = C - A, showing the weight of the composites final product, all mass unit is measured in grams.

The percent yield for solvent variation, categorized as demineralized water (W1–W3), methanol (M1–M3), and acetone (Ac1–Ac3), where the numbers (1–3) represent experimental replicates, is summarized in Table 1, where acetone-based composites exhibited the highest yield among all tested solvents. Interaction between the clay and polar solvents, such as water (W1 – W3), is hindered by the hydrophobic nature of pyrophyllite. However, it possesses stronger interactions with less polar compounds such as methanol (M1 – M3) and acetone (Ac1 – Ac3) (Ali *et al*., 2021). PEG 6000 polymers are usually considered low in polarity despite containing a C–O bond and hydroxyl groups. Acetone is the least polar solvent with a dielectric constant value of 20.7 εr. Since the dielectric constant is proportional to polarity, this will lead to a stronger interaction between acetone and PEG 6000 than between methanol and demineralized water (Ascencio-Media *et al*., 2024; John, 2019; Xochicale-Santana *et al*., 2021). These properties facilitate better interactions and allow possible intercalation of PEG into the clay layers.

One-way ANOVA using SPSS revealed the value of F_{exp} to be 43.7682, and the critical F value is 5.14 at a significance level of 0.05. F_{exp} value exceeds the critical F value, suggesting that at least one treatment is significantly different. The Duncan Multiple Range Test (DMRT) was then applied as a post hoc test for solvent variation, with subset range comparisons of the sample means at a significance level of 0.05. Means within the same subset have no significant difference, while means sitting in different subsets are significantly different from each other.

The result of the DMRT post hoc test is presented in Table 2. Composites prepared with methanol and acetone were not significantly different, as they fall into the same group, but composites prepared with demineralized sit in subset 1, indicating a significant difference. This suggests that the solvent's polarity plays an important role in the yield, since water is the most polar solvent among methanol and acetone. Based on this result, acetone was selected for the heating time variation, as a high yield reflects the optimal interaction between pyrophyllite and PEG, supporting a more stable composite product and minimizing synthesis losses.

Table 2. DMRT post hoc test result on various solvents.

Treatment	N	Subset for alpha = 0.05	
		1	2
Demineralized water	3	26.8195	
Methanol	3		34.7834
Acetone	3		36.2680
Sig.		1	0.2207

Based on the percent yield data presented in Table 3, the sample codes used in this study were designed to systematically represent both the heating time and the experimental replicates. Each code consists of two parts: the first number (1, 2, or 3) indicates the replicate number, while "T" followed by a number denotes the heating duration in hours. For example, 1T1, 2T1, and 3T1 represent the first, second, and third replicates subjected to 1 hour of heating, respectively. Similarly, 1T1.5, 2T1.5, and 3T1.5 correspond to replicates heated for 1.5 hours, while 1T2, 2T2, and 3T2 represent replicates heated for 2 hours.

The T2 sample exhibited the highest percent yield compared to the T1 and T2 samples. This phenomenon may be attributed to the longer heating time, which enhances the mobility of PEG-6000 and allows it to intercalate into the pyrophyllite structure, as the temperature can affect the physical properties of the composites. Longer exposure to the heating process leads to better polymer diffusion, resulting in better intercalation than shorter heating times (Chen *et al*., 2017). However, heating for 1 hour may result in an incomplete evaporation process and inefficient reactions.

Table 3. Percentage yield data as a function of heating time.

Sample	A	B	C	D	E	Yield (%)	Average yield (%)
1T1	21.8476	29.7332	24.7172	7.8856	2.8696	36.3904	36.3536
2T1	23.6999	32.3563	26.7387	8.6564	3.0388	35.1047	
3T1	23.9135	31.7608	26.8614	7.8473	2.9479	37.5658	
1T1.5	22.9664	31.6421	26.1192	8.6757	3.1528	36.3406	36.1557
2T1.5	22.422	30.6741	25.4588	8.2521	3.0368	36.8003	
3T1.5	22.707	30.6688	25.5196	7.9618	2.8126	35.3262	
1T2	22.3791	29.7728	25.2095	7.3937	2.8304	38.2812	37.7239
2T2	23.2733	31.0417	26.1158	7.7684	2.8425	36.5905	
3T2	23.5286	31.7892	26.6924	8.2606	3.1638	38.2999	

*A = Total weight of the petri dish and baking paper, B = Total weight of the petri dish, baking paper and composites mixture before heating process, C = Total weight of the petri dish, baking paper and composite after heating process, D = B-A, showing the weight of the composites mixture, E = C - A, showing the weight of the composites final product, all mass unit is measured in grams.

The one-way ANOVA of the composite sample for heating variation, with each treatment considered an individual group, yielded an F_{exp} value of 2.1537. The critical F value for df_1=2, df_2=6 at a significance level of 0.05 is 5.14. Therefore, $F_{exp}<F_{table,}$ making the null hypothesis not rejected, and there is no significant difference declared. Post hoc analysis was not conducted because the F-statistic indicated no statistically significant

difference. These results indicate that heating for 1, 1.5, or 2 hours does not produce a statistically significant difference in percent yield.

The visual observations of the composites in solvent variations, along with their masses and percent yield, are provided in Table 4. A relatively smooth surface is observed on the composites prepared with demineralized water (W1 – W3) after the heating treatment. Most areas, including the edges, appeared slightly glossy, which suggests less effective interaction between composite components due to the hydrophobicity nature of pyrophyllite and the tendency of hydrogen bonding formation between PEG-6000 and water molecules, since PEG-6000 can act as a hydrogen bonding acceptor, caused by the presence of oxygen in the polymer structure (Ali *et al*., 2021; Fan *et al*., 2016). This phenomenon leads to poor diffusion of PEG into the clay's interlayer structure.

Methanol-based composites (M1 – M3) exhibited visibly rougher surfaces and a non-glossy surface appearance accompanied by a macro-porous structure attributed to the evaporation process, indicating a better intercalation process of PEG into the mineral matrix. Exposure to high temperatures causes composite samples prepared with methanol to undergo harsh evaporation, yielding high porosity and surface irregularity due to methanol's lower boiling point compared to that of demineralized water (Brini *et al*., 2017; Liu *et al*., 2025). Composite samples prepared with acetone (A1 – A3) as the solvent exhibit a surface morphology similar to that of methanol, with higher roughness due to acetone's low boiling point, which causes it to evaporate faster upon contact with high temperatures, leaving a macroporous structure on the composite's surface (Elfasakhany, 2016). A better intercalation process for the composites is suggested, resulting in a non-glossy surface appearance. The decrease in the weight of the composite was observed due to the further drying process during storage in the desiccator.

Table 4. Pictures and weights of the composite before heating, and the final product for each sample on various solvents.

Sample ID	Mass of the composite before heating (g)	Picture of the composite before heating	Picture of the composite after heating	Picture of the composite after 7 days	Mass of the final composite product (g)	Yield (%)
W1	11.7944			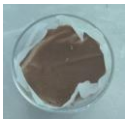	3.0565	25.9148
M1	8.2539		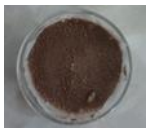	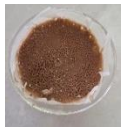	2.8408	34.4177
A1	8.6757		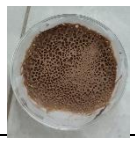		3.1528	36.3406

The visual appearance of the composite samples in Table 5 shows macro-porous surfaces and high irregularity. This is due to acetone's low boiling point, which causes rapid, harsh evaporation from the composite's surfaces (Elfasakhany, 2016). 1T1 – 3T1 samples exhibited the least macro-porous surface compared to 1T1.5 – 3T1.5 samples due to shorter heating time. 1T2 – 3T2 samples demonstrated a more uniformly porous surface structure, with relatively smaller pores, and subtle differences between the variations. Thermal treatment may degrade the composite's structure and volatilize certain components, thereby reducing pore size. However, during prolonged heating, smaller pores can merge, leading to larger pores or even their disappearance (Li *et al*., 2021; Yang and Ye, 2022). The relatively low homogeneity observed in composite samples may be assigned to the minor oxide contents within the clay framework. Oxides, such as potassium oxide, vanadium oxide, and copper oxide, occupying the interlayer space can hinder uniform intercalation of PEG (Shah *et al*., 2024).

Table 5. Pictures and weights of the composite before heating and the final product for each sample at various heating times.

Sample ID	Mass of the composite before heating (g)	Picture of the composite before heating	Picture of the composite after heating	Picture of the composite after 7 days	Mass of the final composite product (g)	Yield (%)
1T1	7.8856		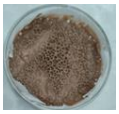	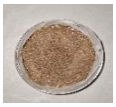	2.8696	36.3904
1T1.5	8.6757		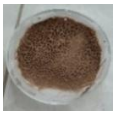		3.1528	36.3406
1T2	7.3937	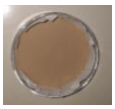			2.8304	38.2812

Melting Point Characterization

One-way ANOVA of heating time indicated no statistically significant difference among T1, T1.5, and T2 samples, although T2 showed the highest percent yield. From an efficiency standpoint, applying a 2-hour treatment is considered excessive if statistical analysis shows no meaningful difference. The result showed a higher melting point with 1 hour of treatment (120.7667 °C) than with 2 hours of heating (116.0333 °C). The melting point data of T1 and T2 samples are shown in Table 6, and to examine the statistical difference between the two means, a T-test was performed. The calculated T-value of 10.356 surpasses the critical T-value of 2.776 (df = 4, α = 0.05). The null hypothesis is rejected, confirming a significant difference in the melting-point behavior of the composite samples. These melting points lie between the melting point of pure pyrophyllite (~1580 °C) and pure PEG 6000 (~60 °C). The difference in melting points between the composite products and the raw material suggests the formation of a new composite material with its own thermal properties, rather than a simple physical mixture, since these values are also affected by the duration of the heating treatment (Ali *et al*., 2021; Altamimi and Neau, 2017). If the PEG existed solely as an unbound polymer, its melting point would be expected to remain unchanged. However, the observed melting points of the composite indicate that PEG has entered an intercalation framework, the stability of which is further affected by thermal exposure.

Extended heating duration may lead to structural alteration and degradation of the composites, such as the breakdown of polymer chains into smaller fragments. This process can disrupt the intercalated clay and weaken the interaction between PEG and pyrophyllite, potentially influencing the thermal stability of the composites and lowering the melting point (Karbhari *et al*., 2021; Ogabi *et al*., 2021).

Table 6. Melting point data analysis of the composites for various heating times.

Sample	Melting point		Average Point	Group Mean	SD
	Initial	Final			
1 hour heating time					
1T1	119.8	120	119.9		
2T1	121	121.2	121.1	120.7667	0.7572
3T1	121.2	121.4	121.3		
2 hours heating time					
1T2	115.8	116	115.9		
2T2	116.2	116.4	116.3	116.0333	0.2309
3T2	115.8	116	115.9		

FTIR Characterization

The IR spectra for 1 and 2 hours of heating are shown in Figure 1. O–H stretching vibration displays peaks in both variations at 3673.92 cm^{-1}. Bands at 3501.35 cm^{-1} in T1 and 3507.05 cm^{-1} in the T2 samples can be attributed to the O–H stretching vibration of the PEG structure, indicating the presence of polymer in the composite samples. The C–H stretching absorption was invariably observed at 2883.8 cm^{-1} in both variations. Similarly, the Al–OH pyrohyllite stretching band at 1146.67 cm^{-1} was consistently present. The presence of PEG was indicated

by C–O stretching at 1101.04 cm^{-1} and 1103.89 cm^{-1} for T1 and T2 samples, respectively. The Si–O–Al stretching peaks at 671.71 cm^{-1}, as well as the AlO_6 octahedral vibration at 450.68 cm^{-1}, are observed in both samples. Those two vibrations belong to the pyrophyllite structure within the composites. Another AlO_6 octahedral peak shows peaks at 536.26 cm^{-1} in the T1 sample and 534.83 cm^{-1} in the T2 sample. The FTIR data analysis uses the first replication for both T1 and T2 samples, since all replications yielded similar wavenumbers and intensities.

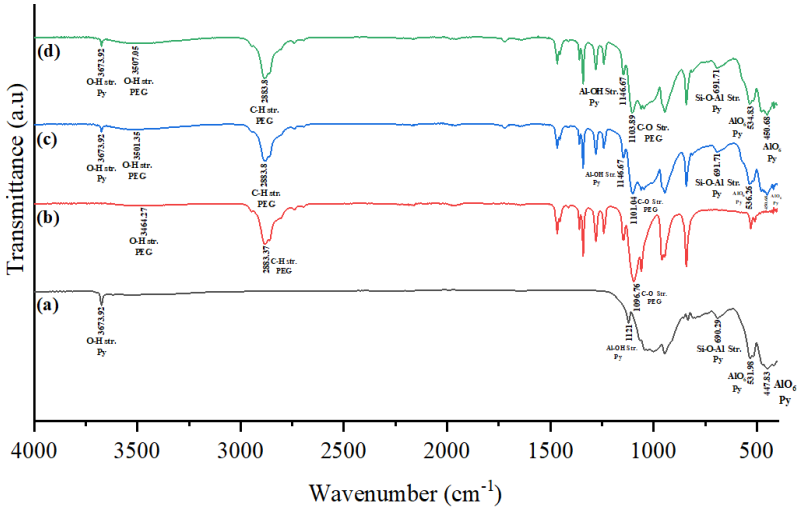

Figure 1. IR spectra result of (a) pyrophyllite, (b) PEG 6000, (c) 1T1, and (d) 1T2

Table 7. FTIR data analysis from raw material and 1-hour treatment composite.

Functional group	Sample	Wavenumber (cm^{-1})	Transmittance (%)
O–H stretching (Al–OH linkage)	Pyrophyllite	3673.92	82.21
	Composite	3673.92	88.56
O–H stretching	PEG 6000	3464.27	96.56
	Composite	3501.35	91.70
C–H stretching	PEG 6000	2882.37	52.75
	Composite	2883.80	52.21
C–O stretching	PEG 6000	1279.31	55.74
	Composite	1279.31	61.01
Si–O stretching	Pyrophyllite	1121.00	61.94
	Composite	1146.67	56.42
Al–OH bending	Pyrophyllite	834.33	65.26
	Composite	841.46	20.54
Si–O–Al bending	Pyrophyllite	531.98	21.46
	Composite	536.26	23.33

The FTIR data comparisons between the raw material and the composites after 1 hour of heating are summarized in Table 7. These functional groups were chosen due to their unique characteristics, providing insights into the chemical interactions and chemical environment within the composite samples. The IR data in Table 7 showed the transmittance rise in the observable peak at 3673.92 cm^{-1} from 82.21% in the raw material to 88.56% for the O–H functional group belonging to pyrophyllite in the samples, indicating a modified chemical environment affecting O–H pyrophyllite in the raw material and the composite (Tsai and Chang, 2024). A wavenumber shift can be observed in the O–H stretching of the composite samples from 3464.27 cm^{-1} in the raw material to 3501.35 cm^{-1} (blueshift), accompanied by a decrease in transmittance from 96.56% to 91.70%. The wavenumber and intensity of the C–H stretching in the composite containing PEG-6000 are relatively constant, indicating no significant chemical changes affecting the C–H bond. Similarly, the C–O stretching of PEG-6000 remained unchanged in intensity, though it was followed by an increase in transmittance from 55.74% to 61.01%. Si–O stretching showed an increase in wavenumber from 1121.00 cm^{-1} to 1146.67 cm^{-1}, followed by a reduction in transmittance from 61.49% to 56.42%. Al–OH bending displayed a wavenumber increase from 834.33 cm^{-1} in the

raw material to 841.46 cm^{-1} (blueshift) in the composite samples. This vibration also showed a transmittance decrease of 65.26% in the raw material to 20.54% in the composite samples. Si–O–Al stretching showed a slight increase in wavenumber (blueshift) from 531.98 cm-1 to 536.26 cm-1, with a small increase in transmittance compared to the raw material, from 21.46% to 23.33%.

The wavenumbers and percent transmittance data for specific functional groups of composites after 2 hours of heating (Table 8) showed that the O–H functional group at 3673.92 cm^{-1}, assigned to the pyrophyllite, increased in transmittance from 82.21% in the raw material to 88.25% in the composite samples. This may indicate the difference in the chemical environment (Tsai and Chang, 2024). O–H stretching band of PEG-6000 structure shifted from 3464.27 cm^{-1} in the raw material to 3507.05 cm^{-1} (blueshift), accompanied by a reduction in transmittance from 96.56% to 91.71%. C–H stretching associated with the PEG-6000 structure showed no significant shift or changes in both wavenumber and percent transmittance. This may indicate no major chemical alteration associated with the C–H bond. The C–O stretching maintained a consistent wavenumber marked by an increase in transmittance from 55.74% to 11.92%. The Si–O stretching vibration of pyrophyllite shifted from 1121 to 1146.67 cm^{-1}, with a modest decrease in transmittance. A reduction in transmittance was observed from the Al–OH bending vibration at 841.46 cm^{-1} from 65.26% to 21.76%. Si–O–Al stretching showed a slight shift in wavenumber (blueshift) from 531.98 cm^{-1} to 534 cm^{-1} with a small decrease in transmittance compared to the raw material from 21.46% to 22.86%.

Table 8. FTIR data analysis from raw material and 2-hour treatment composite.

Functional group	Sample	Wavenumber (cm^{-1})	Transmittance (%)
O–H stretching (Al–OH linkage)	Pyrophyllite	3673.92	82.21
	Composite	3673.92	88.25
O–H stretching	PEG 6000	3464.27	96.56
	Composite	3507.05	91.71
C–H stretching	PEG 6000	2882.37	52.75
	Composite	2883.80	51.99
C–O stretching	PEG 6000	1279.31	55.74
	Composite	1279.31	61.70
Si–O stretching	Pyrophyllite	1121.00	61.94
	Composite	1146.67	56.63
Al–OH bending	Pyrophyllite	834.33	65.26
	Composite	841.46	21.76
Si–O–Al bending	Pyrophyllite	531.98	21.46
	Composite	534.83	22.86

In the aluminosilicate structure, aluminum can act as a Lewis acid, forming a coordination bond with a Lewis base such as OH^-. The oxygen atom of the PEG uses its electron pair to attack the aluminum (Figure 2). This bond can participate in an O–H stretching, giving a more pronounced peak at 3673.92 cm^{-1}. Since the reaction involves an aluminum atom bonded to oxygen, this interaction appears to modify the Si–O–Al group, leading to changes in wavenumber and percent transmittance compared to those of pyrophyllite as the raw material.

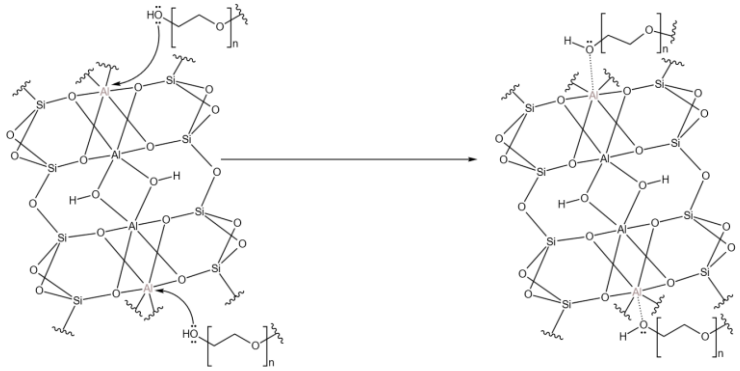

Figure 2. The oxygen of the PEG-6000 interacts with the aluminum of the pyrophyllite.

A difference in the chemical environment can affect the characteristics of a functional group. Oxygen's electronegativity allows it to form hydrogen bonds with other molecules through intermolecular forces. Thus, giving the possibility of the oxygen attached to silicon in the tetrahedral layer to interact with the hydrogen of the OH group belonging to the PEG 6000 structure (Figure 3). This intermolecular interaction between pyrophyllite and PEG 6000 shifts the OH absorption band of PEG 6000 to 3507.05 cm^{-1}, decreasing its percent transmittance. This occurs because the bond is less mobile, thereby lowering the OH vibrational absorption. The Si–O bond will also be less polar, as the electron is drawn to bind to hydrogen on the PEG backbone, limiting bond motion and decreasing its percent transmittance, as observed at 1146.67 cm^{-1}. Figure 5 shows the interaction between oxygen from pyrophyllite and hydrogen from the PEG 6000.

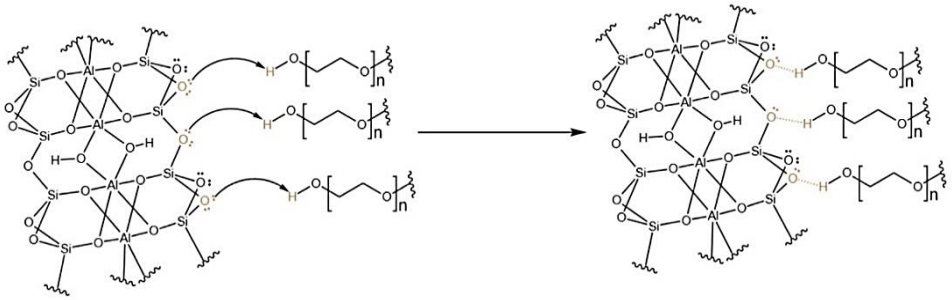

Figure 3. The hydrogen bond formed between the oxygen of the pyrophyllite structure and the hydrogen atom of PEG 6000.

Another possible interaction is a hydrogen bond between the oxygen atom of PEG 6000 and the hydrogen atom of the pyrophyllite structure, as shown in Figure 4. Oxygen uses its lone pair to attack the hydrogen bonded to it within the pyrophyllite. The hydrogen bond formed limits the flexibility of the Al–OH vibration, resulting in a significant decrease in the percent transmittance of Al–OH at 841.46 cm^{-1}.

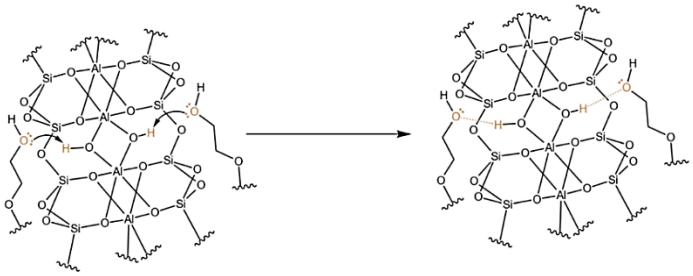

Figure 4. Hydrogen bond interaction between the oxygen of PEG 6000 and the hydrogen from pyrophyllite.

A weak intermolecular interaction can occur between the oxygen atom of the tetrahedral layer in the clay framework and the carbon backbone of PEG 6000 (Figure 5). This weak intermolecular interaction is due to the difference in the electronegativity between oxygen and carbon. The minor electron cloud within the carbon atom of the PEG backbone is pulled to the oxygen of pyrophyllite, which causes the C–O bond of PEG to be more polarized. Such interaction can increase the percent transmittance of C–O stretching vibration at 1279.31 cm^{-1}.

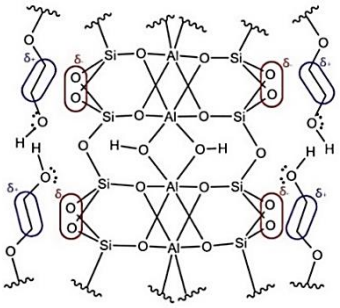

Figure 5. A weak electrostatic interaction between the oxygen of the tetrahedral layer in pyrophyllite and the carbon backbone of PEG.

CONCLUSION

Pyrophyllite-Polyethylene glycol (PEG) 6000 composites were successfully synthesized using the casting method and sol-gel technique. The composite samples with the highest yield (38.2999%) were obtained using acetone as the solvent with a 2-hour heating time. The best performance may be due to the thermal behavior and the interaction between the raw materials and the solvent used. The statistical results revealed a significant difference in percent yield between composite samples prepared with demineralized water and those prepared with other solvents, but no significant difference in various heating times. The composite samples prepared with demineralized water showed a relatively smooth surface compared to other solvents, indicating poor polymer diffusion into the clay structure. Acetone-based composites had the most porous structure among others in solvent variation due to their low boiling point. The 2-hour samples exhibited a more even porous structure than the other variations. Prolonged heating time may cause the pores to merge or shrink. This may also trigger decomposition of the volatile component or structural damage. Melting point characterization using of 1-hour and 2-hours sample resulted in melting point of 120.7667 °C and 116.0333 °C respectively with a significant difference from each other, indicating the successful composite synthesis, this was further confirmed by FTIR analysis with the presence of characteristic functional groups (O–H stretching, 3673.92 cm^{-1}, C–H strectching, 2882.37 cm^{-1}, Al–OH stretching 1146.67 cm^{-1}), indicating some potential interactions between pyrophyllite and PEG.

CONFLICT OF INTEREST

There is no conflict of interest in this article.

AUTHOR CONTRIBUTION

SM: Conceptualization, Methodology, Formulation, Funding, Resources, Supervision, Data Validation, Manuscript Review, and Manuscript Revision; EE: Synthesis, Characterization, Data Analysis, and Manuscript Drafting; RR: Manuscript Review; HK: Manuscript Review.

ACKNOWLEDGEMENT

The authors would like to thank the Chemistry Department and Inorganic Chemistry Laboratory of Brawijaya University for supporting the facilities used in the research.

REFERENCES

Ali, M.A., Ahmed, H.A.M., Ahmed, H.M., and Hefni, M., 2021. Pyrophyllite: An Economic Mineral for Different Industrial Applications. *Applied Sciences (Switzerland)*, 11. https://doi.org/10.3390/app112311357.

Altamimi, M.A., and Neau, S.H., 2017. Investigation of the In Vitro Performance Difference of Drug-Soluplus® and Drug-PEG 6000 Dispersions When Prepared Using Spray Drying or Lyophilization. *Saudi Pharmaceutical Journal*, 25, 419–439. https://doi.org/10.1016/j.jsps.2016.09.013.

Amari, A., Mohammed Alzahrani, F., Mohammedsaleh Katubi, K., Salem Alsaiari, N., Tahoon, M.A., and Ben Rebah, F., 2021. Clay-Polymer Nanocomposites: Preparations and Utilization for Pollutants Removal. *Materials (Basel, Switzerland)*, 14. https://doi.org/10.3390/ma14061365.

Ascencio-Medina, E., He, S., Daghighi, A., Iduoku, K., Casanola-Martin, G.M., Arrasate, S., González-Díaz, H., and Rasulev, B., 2024. Prediction of Dielectric Constant in Series of Polymers by Quantitative Structure-Property Relationship (QSPR). *Polymers*,. https://doi.org/10.3390/polym16192731.

Bîrcă, A., Gherasim, O., Grumezescu, V., and Grumezescu, A.M., 2019. *Chapter 1 - Introduction in Thermoplastic and Thermosetting Polymers*, in: Grumezescu, V., Grumezescu, A.M. (Eds.), Materials for Biomedical Engineering. Elsevier, pp. 1–28. https://doi.org/10.1016/B978-0-12-816874-5.00001-3.

Brini, E., Fennell, C.J., Fernandez-Serra, M., Hribar-Lee, B., Lukšič, M., and Dill, K.A., 2017. How Water's Properties Are Encoded in Its Molecular Structure and Energies. *Chemical Reviews*, 117, 12385–12414. https://doi.org/10.1021/acs.chemrev.7b00259.

Buruga, K., Song, H., Shang, J., Bolan, N., Jagannathan, T.K., and Kim, K.-H.H., 2019. A Review on Functional Polymer-Clay Based Nanocomposite Membranes for Treatment of Water. *Journal of Hazardous Materials*, 379, 120584. https://doi.org/10.1016/j.jhazmat.2019.04.067.

Callister, W.D., and Rethwisch, D.G., 2020. *Fundamentals of Materials Science and Engineering: An Integrated Approach*, Fifth ed. Wiley.

Chen, R.S., Ahmad, S., and Gan, S., 2017. Characterization of Recycled Thermoplastics-Based Nanocomposites: Polymer-Clay Compatibility, Blending Procedure, Processing Condition, and Clay Content Effects.

Composites Part B: Engineering, 131, 91–99. https://doi.org/10.1016/j.compositesb.2017.07.057.

Choudhury, S., 2024. A Review of The Sol-Gel Process and Its Application. *International Education and Research Journal*, 122–125. https://doi.org/10.21276/ierj24449856325648.

Egbo, M.K., 2021. A Fundamental Review on Composite Materials and Some of Their Applications in Biomedical Engineering. *Journal of King Saud University - Engineering Sciences*, 33, 557–568. https://doi.org/10.1016/j.jksues.2020.07.007.

Elfasakhany, A., 2016. Performance and Emissions Analysis on Using Acetone–Gasoline Fuel Blends in Spark-Ignition Engine. *Engineering Science and Technology, an International Journal*, 19, 1224–1232. https://doi.org/10.1016/j.jestch.2016.02.002.

Essalhi, A., Essalhi, M., Toummite, A., Mostadi, A., Raddi, Y., El Mostadi, A., and Raddi, Y., 2017. Mineralogical and Textural Arguments for a Metasomatic Origin of the Ougnat Pyrophyllite, Eastern Anti-Atlas, Morocco. *Journal of Materials and Environmental Science*, 8, 22–32.

Et-tanteny, R., El Amrani, B., Manssouri, I., and Limami, H., 2024. Physicochemical, Mechanical and Thermal Analysis of Unfired Clay Bricks: Kaolinite-PEG 6000 Composite. *Cleaner Engineering and Technology*, 22, 100793. https://doi.org/10.1016/j.clet.2024.100793.

Fan, X., Su, Y., Zhao, X., Li, Y., Zhang, R., Ma, T., Liu, Y., and Jiang, Z., 2016. Manipulating the Segregation Behavior of Polyethylene Glycol by Hydrogen Bonding Interaction to Endow Ultrafiltration Membranes with Enhanced Antifouling Performance. *Journal of Membrane Science*, 499, 56–64. https://doi.org/10.1016/j.memsci.2015.10.026.

Gaballa, sherif A., Naguib, Y., Mady, F.M., Khaled, K.A., Armia, S., Naguib, Y., Mady, F.M., Khaled, K.A., Gaballa, sherif A., Naguib, Y., Mady, F.M., and Khaled, K.A., 2024. Polyethylene Glycol: Properties, Applications, and Challenges. *Journal of advanced Biomedical and Pharmaceutical Sciences*, 7, 26–36. https://doi.org/10.21608/jabps.2023.241685.1205.

Helsinta, N., Halim, A., Octavia, M.D., and Rivai, H., 2021. Review: Solid Dispersion of Fenofibrate Using Poly Ethylene Glycol 6000. *International Journal of Pharmaceutical Sciences and Medicine*,. https://doi.org/10.47760/ijpsm.2021.v06i06.005.

John, A.O., 2019. The Role of Solvents' Dielectric Constants in the Delicate Interplay between Microstructure and Optical Properties of Poly (3-Hexylthiophene) Thin Films. *American Journal of Nanoscience and Nanotechnology Research*, 7, 1–13.

Karbhari, V.M., Xian, G., and Hong, S., 2021. Effect of Thermal Exposure on Carbon Fiber Reinforced Composites Used in Civil Infrastructure Rehabilitation. *Composites Part A: Applied Science and Manufacturing*, 149, 106570. https://doi.org/10.1016/j.compositesa.2021.106570.

Kridli, G.T., Friedman, P.A., and Boileau, J.M., 2021. *Chapter 7 - Manufacturing Processes for Light Alloys*. Updated by J.M. Boileau and P.K. Mallick., in: Mallick, P.K. (Ed.), Materials, Design and Manufacturing for Lightweight Vehicles (Second Edition), Woodhead Publishing in Materials. Woodhead Publishing, pp. 267–320. https://doi.org/10.1016/B978-0-12-818712-8.00007-0.

Li, T., Wu, J.J., Wang, X.G., and Huang, H., 2021. Particle Size Effect and Temperature Effect on the Pore Structure of Low-Rank Coal. *ACS Omega*, 6, 5865–5877. https://doi.org/10.1021/acsomega.0c06280.

Liu, Z., Yin, Z., Cox, C., Bosman, M., Qian, X., Li, N., Zhao, H., Du, Y., Li, J., and Nocera, D.G., 2025. Room Temperature Stable CO_x-Free H_2 Production from Methanol with Magnesium Oxide Nanophotocatalysts. *Science Advances*, 2, e1501425. https://doi.org/10.1126/sciadv.1501425.

Martadiastuti, V., Winarno, T., Ali, R.K., and Purba, E.C., 2024. Characteristics of Pyrophyllite and Hydrothermal Alteration at Argotirto Area, Malang Regency, East Java, Indonesia. *IOP Conference Series: Earth and Environmental Science*, 1378, 12027. https://doi.org/10.1088/1755-1315/1378/1/012027.

Mutrofin, S., Setyaningsih, T., Wati, F., and Purwonugroho, D., 2018. Physical-Chemistry of Nawangan's Phyropyllite and Its Prospective as Environmental Friendly Geopolymer Materials. *IOP Conference Series: Materials Science and Engineering*, 285, 12026. https://doi.org/10.1088/1757-899X/285/1/012026.

Ogabi, R., Manescau, B., Chetehouna, K., and Gascoin, N., 2021. A Study of Thermal Degradation and Fire Behaviour of Polymer Composites and Their Gaseous Emission Assessment. *Energies*,. https://doi.org/10.3390/en14217070.

Shah, N., Shah, M., Khan, F., Rehan, T., Shams, S., Khitab, F., Khan, A., Ullah, M.W., Yousaf, J., Awwad, F.A., and Ismail, E.A.A., 2024. Fabrication and Characterization of Montmorillonite Clay/Agar-Based Magnetic Composite and Its Biological and Electrical Conductivity Evaluation. *ACS Omega*, 9, 15904–15914. https://doi.org/10.1021/acsomega.3c08708.

Tsai, T.-H.H., and Chang, P.-P.P., 2024. A Study on the Conductivity and Infrared Spectroscopy of Elastic Polymer Composite Materials. *Applied Sciences*, 14. https://doi.org/10.3390/app14177899.

Wang, S., Gainey, L., Mackinnon, I.D.R., Allen, C., Gu, Y., and Xi, Y., 2023. Thermal Behaviors of Clay Minerals as Key Components and Additives for Fired Brick Properties: A Review. *Journal of Building Engineering*, 66, 105802. https://doi.org/10.1016/j.jobe.2022.105802.

Xochicale-Santana, L., Vidyasagar, C.C., Muñoz-Flores, B.M., and Pérez, V.M.J.J., 2021. *Chapter 15 - Microwave Assisted Organic Syntheses (MAOS): The Green Synthetic Method*, in: Kharisov, B., Kharissova, O. (Eds.), Handbook of Greener Synthesis of Nanomaterials and Compounds. Elsevier, pp. 491–542. https://doi.org/10.1016/B978-0-12-821938-6.00015-3.

Yang, H., and Ye, F., 2022. Microtexture, Microstructure Evolution, and Thermal Insulation Properties of Si3N4/Silica Aerogel Composites at High Temperatures. *RSC Advances*, 12, 12226–12234. https://doi.org/10.1039/d2ra01336c.